INTERNATIONAL JOURNAL OF CLIMATOLOGY
Int. J. Climatol. (2015)
Published online in Wiley Online Library
(wileyonlinelibrary.com) DOI: 10.1002/joc.4536

RMetS
Royal Meteorological Society

Atmospheric drought in Belgium – statistical analysis of precipitation deficit

Sepideh Zamani,[a] Anne Gobin,[b] Hans Van de Vyver[a]* and Jeroen Gerlo[a]

[a] *Meteorological and Climatological Research, Royal Meteorological Institute, Brussels, Belgium*
[b] *Flemish Institute for Technological Research, Mol, Belgium*

ABSTRACT: The principle of return periods or frequencies of natural hazards is adopted in many countries as the basis of eligibility for the compensation of associated losses. For adequate risk management and eligibility in Belgium, hazard maps for drought events with a 20-year return period are needed. The maximum precipitation deficit in the summer half-year (1 April–30 September) was taken as a good indicator for atmospheric drought severity during a particular year. Precipitation deficit is calculated as a cumulative balance between precipitation and evapotranspiration for a free open water surface, short grass, deciduous forest and coniferous forest. Precipitation deficit maxima were modelled with the generalized extreme value (GEV) distribution. Mapping precipitation deficit return levels is based on a GEV distribution where the parameters vary smoothly in space as a function of altitude and distance to the sea. The final products are return level maps of extreme precipitation deficit, relevant for insurance companies providing cover for the forestry and agriculture sector.

KEY WORDS drought; precipitation deficit; generalized extreme value (GEV) distribution; return level mapping

Received 12 January 2015; Revised 15 September 2015; Accepted 16 September 2015

1. Introduction

During the last century, drought events have had marked influences on forest and agricultural ecosystems in Europe (Olesen and Bindi, 2002; Maracchi *et al.*, 2005; Orlandini *et al.*, 2008; Reidsma *et al.*, 2009). In general, drought is considered as an extended period of deficiency in water supply (Beran and Rodier, 1985; Rossi, 2000). Drought is a complex phenomenon which is difficult to monitor. The absence of a precise and universally accepted definition adds to the confusion whether or not a drought exists, and if it does, what its degree of severity is. Some droughts can persist for several years, and even short, intense droughts can cause significant damage and harm to the local economy. The spatio-temporal complexity of drought makes it more difficult to establish a threshold for each level of severity, and these thresholds should be associated with the anticipated damages (economic, agricultural, social, etc.) that a drought may exert on a certain region. Based on a thorough review of drought definitions (Dracup *et al.*, 1980; Wilhite and Glantz, 1985), six different drought categories are identified: meteorological, climatological, atmospheric, agricultural, hydrological and water management. Meteorological droughts, for example, defined as precipitation shortage in absolute amounts for a given period, often occur in Belgium (Brouyaux *et al.*, 2008). However, more relevant to vegetation is atmospheric drought, which is defined not only in terms of precipitation shortages but also in terms of temperature, humidity and wind speed.

A wide range of literature exists on the issue of drought estimations at specific locations (Beran and Rodier, 1985; Tallaksen and Hisdal, 1997; Hisdal *et al.*, 2001), but not many studies deal with the spatial estimation of drought risk. As droughts are regional in nature and commonly cover large areas and extended time periods, it is important to study such events within a regional context. Regional drought analyses are often based on single site event definitions where the areal aspect is included by studying the spatial pattern without introducing a separate, regional drought event definition. Different approaches to regional drought analyses have been reviewed by Rossi *et al.* (1992), applying lack of precipitation as an example.

Extreme value theory (EVT) (Coles, 2001; Beirlant *et al.*, 2004) characterizes the behaviour of extreme observations. A reliable prediction of the likelihood of rare but plausible events, allows EVT to be applicable in many domains of environmental research, e.g. climate (Naveau *et al.*, 2005), hydrology (Katz *et al.*, 2002), soil analysis (Goegebeur *et al.*, 2005). One of the most important methodologies in EVT is block-maxima methods, which model the largest values collected from large samples of observations. A major result of EVT is that the generalized extreme value (GEV) distribution is the only possible limit distribution of properly normalized maxima of a sequence of independent and identically distributed (iid) random variables. The tail behaviour of the GEV

* Correspondence to: H. Van de Vyver, Royal Meteorological Institute of Belgium, Meteorological and Climatological Research, Ringlaan 3, 1180 Brussels, Belgium. E-mail: hvijver@meteo.be

distribution allows for the estimation of return levels for associated return periods considerably beyond the end of the data to which the model is fitted.

A large part of this article is devoted to the problem of how to model the spatial characteristics of extreme precipitation deficit, and its spatial mapping on the basis of EVT. In general, the problem of mapping return levels of a certain climatological variable involves the definition of marginal distributions at single sites, and subsequently translating the distribution parameters to a regional level using spatially continuous variables. Spatial GEV modelling allows to predict extreme events at locations for which no observations have been available. The advantage of the spatial GEV modelling approach is that it can be used to consider problems concerning the aggregation of regional processes over a country, and interpolation within a region can be accomplished, e.g. for extreme rainfall (Gellens, 2002; Cooley *et al.*, 2007; Sang and Gelfand, 2009; Padoan *et al.*, 2010; Westra and Sisson, 2011; Van de Vyver, 2012; Dyrrdal *et al.*, 2015), snow depth (Blanchet and Lehning, 2010) and hurricane-induced wave heights (Northrop and Jonathan, 2011).

With more than 50% coverage of the Belgian territory, forestry and agriculture represent important drought impact sectors. The Government Disaster Fund is designed to compensate losses associated with a 20-year return period and beyond. In line with this demand, the major objectives of this study are (i) to quantify drought in terms of precipitation deficit, (ii) to investigate whether EVT is applicable to extreme precipitation deficit, and (iii) to determine spatial return levels of extreme precipitation deficit, relevant for insurance companies providing cover for the forestry and agriculture sector.

2. Climatological methods

2.1. Precipitation deficit as a drought indicator

Summer drought may have a negative influence on vegetation growth in Belgium. The potential evapotranspiration (PET) rate has been widely used as an estimate of vegetation water requirements (Williams *et al.*, 2012), and as part of an index in defining the aridity of a climate (Kingston *et al.*, 2009). *Precipitation deficit* is defined as the cumulative difference between daily PET and daily precipitation. When the precipitation deficit becomes negative it is reset to zero. Around early April the average daily evapotranspiration becomes larger than the average daily precipitation; a deficit can therefore accumulate from April onwards. After September, the precipitation deficit tends to decrease as evapotranspiration reduces and rainfall increases. In the Netherlands, the precipitation deficit is defined as the cumulative difference between precipitation and evaporation from April to September (Beersma and Buishand, 2004, 2007). In line with the approach of the Food and Agricultural Organization of the United Nations (FAO) to defining the daily precipitation deficit during the growing season (FAO, 1978), we halve the evapotranspiration rate so that we do not overestimate the occurrence of drought stress:

$$\mathrm{PD} = \frac{1}{2} \times \mathrm{PET} - P \tag{1}$$

where PET is the daily potential evapotranspiration (mm), and P is the daily precipitation (mm). The precipitation deficit maxima is the largest daily precipitation deficit during the year which for each station and each year occurs during the summer half-year (1 April–30 September).

PET has been estimated using the Bultot method (Bultot and Dupriez, 1973; Bultot *et al.*, 1983, 1988), which is developed specifically for Belgium. The Bultot method modifies the Penman equation (Penman, 1948) to estimate reference *daily evaporation*, E_0 (mm), for a free and open water surface, and the Monteith equation for net terrestrial radiation (Monteith, 1973). The daily PET of a natural surface such as an open water surface, grass, deciduous forest and coniferous forest, is subsequently derived from an analytical expression containing the natural surface reflection coefficient (Monteith, 1973; Bultot *et al.*, 1983).

2.2. Data and climate

Belgium has a temperate maritime climate influenced by the North Sea and Atlantic Ocean, with cool summers and mild winters. Because the country is small and predominantly flat, there is little variation in climate from region to region, although the marine influences are less inland. Rainfall is distributed throughout the year with a drier period from April to September. Breezy conditions occur more in the winter than in the summer, and more among the coastal areas than inland. The hills of the eastern regions cause a cooler and wetter climate with more rainfall. The Köppen–Geiger climate classification is Cfb: the warmest month is lower than 22° C on average and 4 or more months are above 10° C on average.

All data were collected by the Royal Meteorological Institute (RMI) of Belgium. At Uccle (50°47′55″ N, 4°21′29″ E, 100 m a.s.l.), all variables necessary for calculating PET of free open water surfaces and grass were registered on a daily basis for 105 years between 1901 and 2005 (Bleiman, 1976). Daily precipitation values (0:00–0:00 UTC) are available for a 116-year period from 1898 onwards (Demarée, 2003). Daily PET-series were calculated for open water surface, grass, coniferous and deciduous forest, for the period 1967–2005 for 12 additional stations across the country (Gellens-Meulenberghs and Gellens, 1992), see Table 1 and Figure 1. The same stations provide daily precipitation measurements during the same period. In 2006, the instruments were replaced by automatic weather stations. The latter measurements are not considered in the study, because the series are not long enough for an extreme value analysis.

In contrast with the Uccle series, some stations display long periods with missing data for both precipitation and PET. Despite this drawback, the network provides important information on regional differences in PET. In obtaining annual maxima precipitation deficit series, the years containing more than 10% missing values (either from precipitation or PET data sets) in the summer half-year were not considered.

Table 1. Characteristics of the 13 stations (cf. Figure 1): altitude, mean annual PET (mm) for open water surface, mean annual precipitation (mm) and the number of annual maxima (AM) precipitation deficit.

	Station	Alt (m)	PET	Precipitation	# AM
1	Koksijde	5	773.5	678.3	32
2	Melle	17	704.6	703.8	39
3	Mol	23	671.7	694.4	26
4	Uccle (water and grass)	100	683.2	822.8	105
	Uccle (forest)				39
5	Wasmuel	25	672.2	691.3	31
6	Ernage	159	693.2	728.3	29
7	Forges	318	661.4	1013.8	33
8	Bierset	191	706.6	843.1	38
9	Spa	483	731.9	1120.6	35
10	Rochefort	193	654.1	739.7	33
11	Carlsbourg	408	653.1	1192.1	19
12	St Hubert	556	681.8	1074.1	38
13	Lacuisine	298	624.4	1113.2	32

The mean annual values were calculated for the available years, except for Uccle, where the mean annual precipitation was calculated for 1967–2005, instead of 1898–present.

3. Statistical methods

3.1. Probability distribution for precipitation deficit maxima

One of the most important methodologies in EVT is concerned with the statistical behaviour of block maxima (Coles, 2001; Beirlant *et al.*, 2004), i.e.

$$M_m = \max\left\{X_1, \ldots, X_m\right\} \tag{2}$$

where $X_1, \ldots, X_m$ is a sequence of independent and iid random variables. In practice, $X_1, \ldots, X_m$ is, for instance, a time series of daily precipitation (Katz *et al.*, 2002). In this work, X_j is related to the precipitation deficit at the jth day in the summer half-year, as defined in Section 2.1. The summer half-year maximum precipitation deficit corresponds with M_m and block size $m = 183$. A key result is that, under regularity conditions, $\Pr\{M_m \leq z\}$ can be approximated by the GEV distribution for large m-values. This is a three-parameter family of functions

$$G(z;\mu,\sigma,\xi) = \exp\left[-\left(1+\xi\frac{z-\mu}{\sigma}\right)^{-1/\xi}\right] \tag{3}$$

where the location-parameter (μ) specifies the centre of the distribution; the scale-parameter (σ) determines the size of deviations in the location parameter; and the shape-parameter (ξ) governs the tail behaviour of the distribution. For sufficiently long time series, it is customary and convenient to extract the block maxima, generating a *block maxima-series*. Pragmatic considerations often lead to the adoption of 1 year blocks, but monthly or seasonal maxima are also considered (Katz *et al.*, 2002).

The GEV-distribution was fitted to the block maxima-series by the maximum likelihood estimator (MLE). For a given sample $\mathbf{z} = (z_1, \ldots, z_k)^T$ of iid GEV random variables, the log-likelihood function is

$$l(\psi) = \sum_{i=1}^{k} \log g\left(z_i;\psi\right) \tag{4}$$

with $\psi = (\mu,\sigma,\xi)$ the vector of GEV-parameters, and $g(z;\psi)$ the probability density function. The MLE $\hat{\psi}$ is obtained by maximizing the log-likelihood function with respect to ψ. Function fit.gev in R-package ismev (Stephenson, 2012), for example, performs MLE.

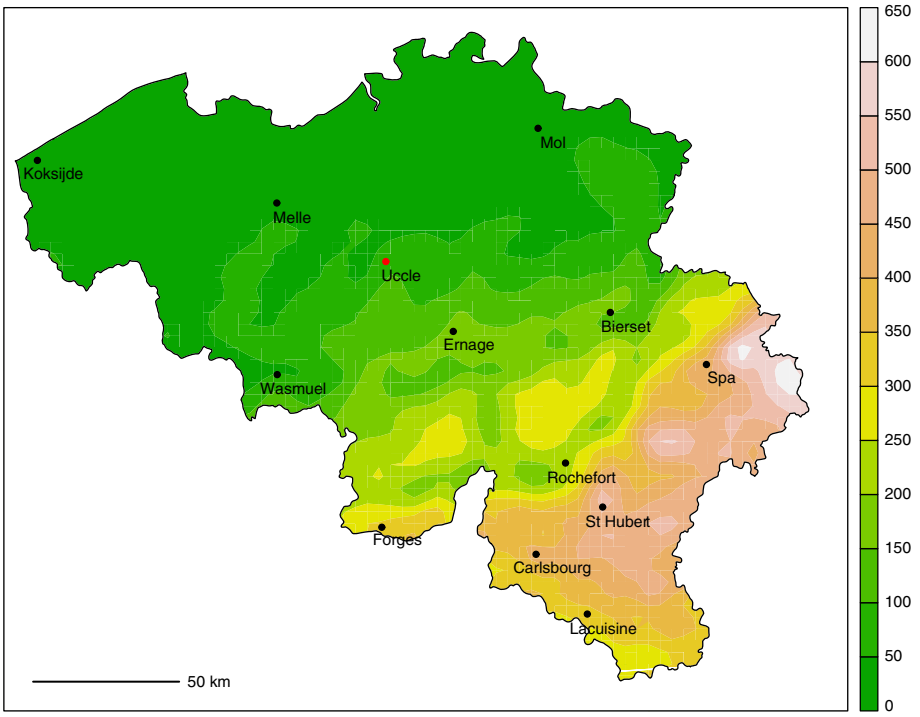

Figure 1. Elevation map (m) of Belgium, together with the position of the 13 stations where the PET-series were obtained.

An easy-to-understand measure of extreme events is the return level. The *return period T* associated with the *return level* z_T is defined as the average period of time between exceedances of z_T:

$$T = \frac{1}{1 - G\left(z_T\right)} \tag{5}$$

see Coles (2001), Beirlant *et al.* (2004). Conversely, the return level z_T is defined as a value which, on average, is exceeded once in T years. This is obtained by inverting Equation (5):

$$z_T = \mu - \frac{\sigma}{\xi}\left\{1 - \left[-\log\left(1 - \frac{1}{T}\right)\right]^{-\xi}\right\} \tag{6}$$

3.2. Spatial mapping of precipitation deficit maxima

The assessment of ecosystem vulnerability to water deficit requires a regional drought analysis. However, estimating the return level of extreme meteorological events is difficult because of limited temporal records. This means that we need to interpolate the distributions to locations where observations are not available. Isoline maps are extensively used to analyse the most severe historical droughts (Rossi *et al.*, 1992). Here we discuss a technique for mapping extreme precipitation deficit on the basis of EVT. Let $X_j(r)$ denote the cumulative precipitation deficit at day j, and at location r (expressed in longitude/latitude, or other geographic coordinates). Let $M_m(r)$ denote the precipitation deficit maximum at location r:

$$M_m(r) = \max\left\{X_1(r), \ldots, X_m(r)\right\}. \tag{7}$$

The main goal of spatial estimation of extremes is to provide inference for the probability $P\{M_m(r) < z\}$ for all locations r within a certain region, in our case Belgium.

3.2.1. *Smooth spatial GEV modelling*

The spatial GEV model of $M_m(r)$ is given by

$$M_m(r) \sim \text{GEV}\left[\mu(r), \sigma(r), \xi(r)\right], \tag{8}$$

where the parameters $\mu(r)$, $\sigma(r)$ and $\xi(r)$ are modelled as a function of explanatory variables, hereafter referred to as spatial covariates. Examples of such covariates are elevation and longitude/latitude. Once the spatial GEV-parameters $\mu(r)$, $\sigma(r)$ and $\xi(r)$ are estimated, and covariate information is available on a dense grid, return level maps can be plotted easily using Equation (6).

Let η denote one of the GEV-parameters. We model $\eta(r)$ as a linear relationship with spatial covariates $C_1(r), \ldots, C_p(r)$:

$$\eta(r) = \eta^{(0)} + \sum_{i=1}^{p} \eta^{(i)} C_i(r). \tag{9}$$

Because the shape parameter ξ determines the nature of the tail of the GEV-distribution, its value has a significant influence on the severity of very extreme events. Unfortunately, no matter what model and estimation method are selected, this parameter is difficult to estimate, especially for data records of relatively short length. A commonly used assumption in the spatial modelling of GEV parameters is that $\xi(r) = \xi$ is constant over relatively small study regions (Gellens, 2002; Cooley *et al.*, 2007; Sang and Gelfand, 2009; Blanchet and Lehning, 2010; Padoan *et al.*, 2010; Northrop and Jonathan, 2011; Westra and Sisson, 2011; Van de Vyver, 2012; Dyrrdal *et al.*, 2015).

3.2.2. *Model estimation and selection*

Inference was done by maximization of the log-likelihood which includes multi-site data. Let the response z_{ij} be the maximum precipitation deficit at the ith site in year j, and r_i be the coordinate of the ith site. For a given sample of spatial data $z = (z_{ij})$ of iid random variables from a GEV-model, Equation (9), an extension of the standard log-likelihood, Equation (4), is:

$$l(\psi) = \sum_{i=1}^{n}\sum_{j=1}^{k} \log\, g\left(z_{ij}; \mu\left(r_i\right), \sigma\left(r_i\right), \xi\right), \tag{10}$$

where $\psi = \left(\mu^{(0)}, \mu^{(1)}, \ldots, \mu^{(p_\mu)}, \sigma^{(0)}, \sigma^{(1)}, \ldots, \sigma^{(p_\sigma)}, \xi\right)$ is the vector of parameters, and $g(z)$ is the density of the GEV-distribution, Equation (3). The MLE $\hat{\psi}$ is obtained by maximizing the log-likelihood function with respect to ψ. Special attention was paid to the spatial dependence between the station data. The asymptotic properties of the independence MLE are well known, but this is not the true model, because spatial data are often highly correlated. A solution to account for dependence is ignoring the dependence initially, thus working with MLE under misspecification, and then making adjustments to estimates of parameter uncertainty (Rotnitzky and Jewell, 1990; Chandler and Bate, 2007; Zheng *et al.*, in press). More precisely, one has

$$\hat{\psi} \to N\left(\psi_0, I\left(\psi_0\right)^{-1} V\left(\psi_0\right) I\left(\psi_0\right)^{-1}\right), \quad \text{as} \quad n \to \infty, \tag{11}$$

where ψ_0 is the vector of true parameters, $V(\psi_0) = \text{Cov}\left[\nabla l(\psi_0)\right]$, and $I(\psi_0) = -E\left[\nabla^2 l(\psi_0)\right]$ the Fisher information matrix (∇ and ∇^2 denote the gradient and Hessian, respectively). The information matrix $I(\psi_0)$ is approximated by $I\left(\hat{\psi}\right)$, which has been included in the standard output of optimisation routines. The estimation of $V(\psi_0)$ poses more difficulties, because the naive estimator $V\left(\hat{\psi}\right)$ disappears when evaluated at the MLE. A more detailed discussion on the estimation of $V(\psi_0)$ may be found in Varin (2008).

Model selection criteria are needed to decide which of the fitted models should be preferred. We used the *Takeuchi Information Criterion*, TIC (Takeuchi, 1976), defined as:

$$\text{TIC} = -2l\left(\hat{\psi}\right) + 2\,Tr\left(I\left(\hat{\psi}\right)^{-1} V\left(\hat{\psi}\right)\right), \tag{12}$$

where $l\left(\hat{\psi}\right)$ is the maximized log-likelihood, Equation (10). TIC is the AIC criterion extended to a misspecified likelihood function. As with the AIC, the best model has the lowest TIC value.

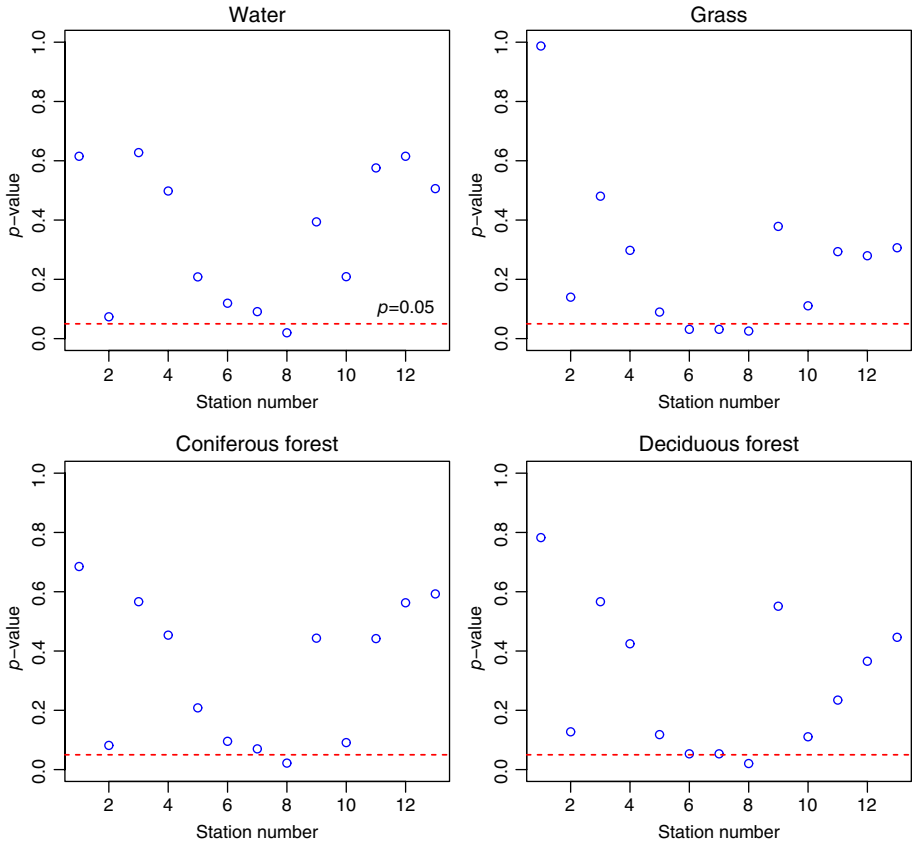

Figure 2. p-Values of Mann–Kendall test statistics for trends in maximum precipitation deficit series. Station number as in Table 1.

4. Results

4.1. Stationarity, time-independence and spatial correlation

A central assumption in this study is that the precipitation deficit maxima are stationary in time. The Mann–Kendall test (McLeod, 2011), which provides information on the presence of tendencies, was applied to the maxima time series (52 in total). The p-values range between 0.019 and 0.987, 46 of them are larger that 0.05 (Figure 2), and indicate that the stationarity of the maxima series is a likely hypothesis. The four maxima series of Bierset (station 8) give p-values smaller than 0.05, and range between 0.019 and 0.025. In addition, maxima series of Ernage and Forges (stations 6 and 7), for cover type grass, give a p-value of 0.031. Owing to the limited time series of PET-data, we decided to include all the series in the analysis.

Another important assumption when modelling individual GEV distributions with log-likelihood, Equation (4), is the time-independence of the maxima series. This can be tested with a plot of the autocorrelation function, as shown for the maximum precipitation deficit of grass at Uccle (Figure 3). The autocorrelation was computed for lags ranging between 1 and 20, and lies within the 95% confidence bounds, which are based on an uncorrelated series. The hypothesis of time-independence can therefore be accepted at the 5% significance level. Similar results were obtained for the other series.

Spatial extremes are modelled assuming that the precipitation deficit maxima are independent in space. This assumption is, of course, not met in reality, as shown by the pairwise Pearson correlation test: the hypothesis that the true correlation coefficient is equal to 0 is rejected for every pair of precipitation deficit maxima series. The p-values are at highest 0.004 (water), 0.007 (grass), 0.005 (coniferous forest) and 0.005 (deciduous forest). In addition, the spatial correlation matrix for water yields values between 0.5 and 1.0, indicating a strong spatial dependence. In Section 3.2.2. we explained how we obtained adjusted inference under this model misspecification.

4.2. Single site distribution

The Uccle observations offer a valuable dataset for studying trends. The plot of the maximum precipitation deficit for grass shows that the driest years 1911, 1921, 1959 and 1976 have above normal precipitation deficit maxima (Figure 4), whereas the lowest deficits were reached in the years 1904, 1920, 1930 and 1948. A 30-year moving average displays no visible temporal trend in precipitation deficit maxima (Figure 4), which is in accordance with the statistical trend tests carried out (see Section 4.1). The GEV distribution, Equation (3), was fitted to the maximum precipitation deficit, and the parameters of the distribution were estimated by MLE. This leads to the estimate

$$\widehat{\mu} = 31.02\ (1.30)\,,\ \widehat{\sigma} = 11.80\ (1.07)\,,\ \widehat{\xi} = 0.253\ (0.083)\,, \tag{13}$$

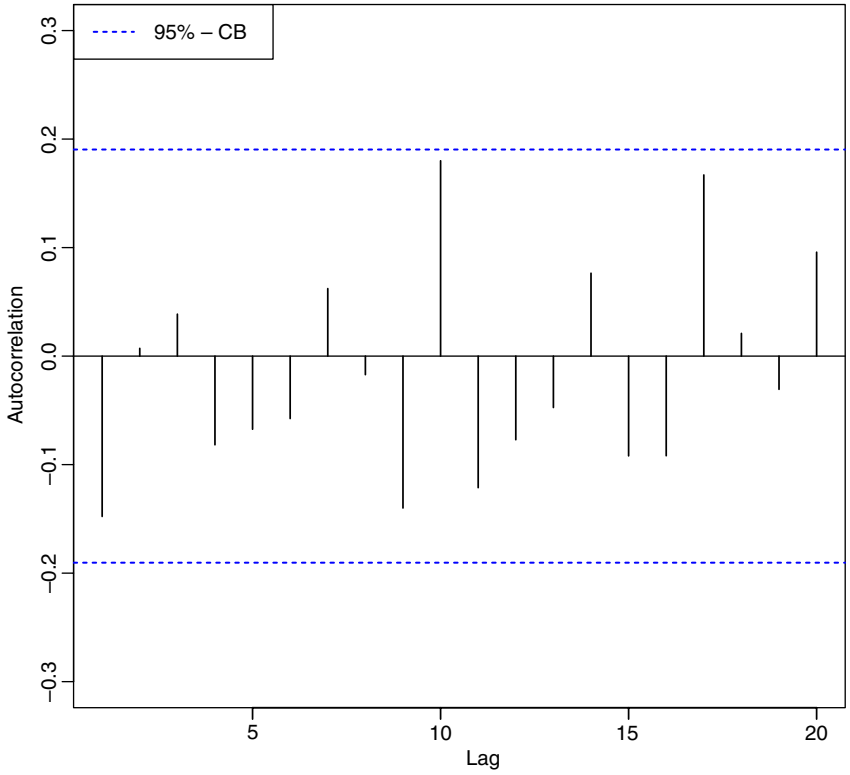

Figure 3. Autocorrelation for maximum precipitation deficit at Uccle (grass).

where the values within the parentheses are the corresponding standard errors.

For a good fit of the GEV model, the points of the quantile plot should lie close to the unit diagonal. The quantile plots for Uccle (Figure 5, top left) demonstrates the validity of the fitted model. Similarly, MLE was performed on the other series (Figure 6, cover type: deciduous forest), and the quantile plots were analysed (Figure 5). We have also considered the station Mol with the worst fit, as there is a strong departure from linearity for the 9 highest annual maxima. We used the Cramer-von Mises goodness-of-fit test for extreme value distributions (Laio, 2004). The p-values are larger than 0.05 (Figure 7), supporting the probable hypothesis that the maxima follow the GEV distribution. As expected, station Mol has the lowest p-value, around $p = 0.1$. In conclusion, there are enough grounds to support the use of the GEV model.

4.3. Modelling spatial data

Suitable covariates were sought to explain a large part of the spatial patterns in the extremes. For spatial mapping, covariate information is needed at regular grid points within the entire region. We focus on four readily available geographical covariates: longitude/latitude, LON/LAT (decimal form), elevation, H (m) and distance to the sea, D (km). For extreme precipitation, several authors confirmed that mean annual rainfall is a stronger covariate than elevation (Cooley *et al.*, 2007; Van de Vyver, 2012). Therefore we introduced the climatological covariate mean summer rainfall, MSR (mm). The MSR was computed over the years 1967–2005, which is also the period of the annual maxima series. Extensive statistical testing (not shown) supports the use of combined covariates, and in particular $\sqrt{D/\mathrm{MSR}}$. Throughout this work, this is referred to as a composite covariate. The composite covariate, $\log(D)+H$, was used to interpolate Makkink evaporation in the Netherlands (Hiemstra and Sluiter, 2011). This covariate did not lead to satisfactory results in our case, because Belgium has a more complex topography than the Netherlands. Because there is a strong linear correlation between MSR and H ($\mathrm{MSR} = a_0 + a_1 H$, with $a_0 = 337.98$, $a_1 = 0.39$, with a correlation ≈ 0.95), an alternative covariate to $\sqrt{D/\mathrm{MSR}}$ was found to be $\sqrt{D/\left(a_0 + a_1 H\right)}$. In what follows, we use the latter composite covariate because gridded values of H and D are available at a regular grid, whereas MSR-values are obtained by spatial interpolation.

An exploratory analysis to assess the influence of a covariate on the GEV-parameters was based on scatter plots. For example, Figure 8 shows the MLEs $\widehat{\mu}_i$, $\widehat{\sigma}_i$ and $\widehat{\xi}_i$ of the ith station, against covariates: distance to the sea, elevation and the composite covariate. It appears that $\widehat{\mu}_i$, $\widehat{\sigma}_i$ are correlated with the covariates, whereas no correlation was found for $\widehat{\xi}_i$. For all the covariates, no obvious inter-site differences in $\widehat{\xi}_i$ were discernible, and this leads to the model assumption $\xi(r) = \xi_0$.

Smooth spatial GEV models $\mathrm{GEV}\left[\mu(r), \sigma(r), \xi(r)\right]$, Equation (9), were estimated by MLE for different covariates (see Section 3.2.2.). The models we compared are listed in Table 2. M_0 is the GEV-model with constant parameters. Models M_1, …, M_5 include a covariate in

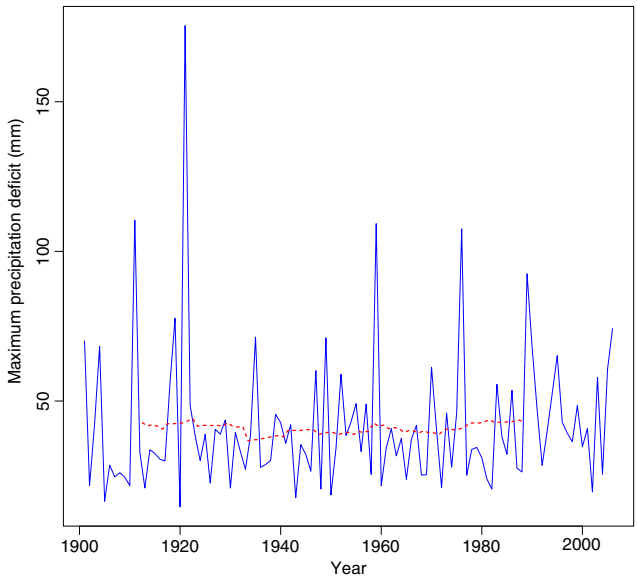

Figure 4. Maximum precipitation deficit (mm) for grass in the summer half-year (1 April–30 September) at Uccle (1901–2005). Dashed line: 30-year moving average.

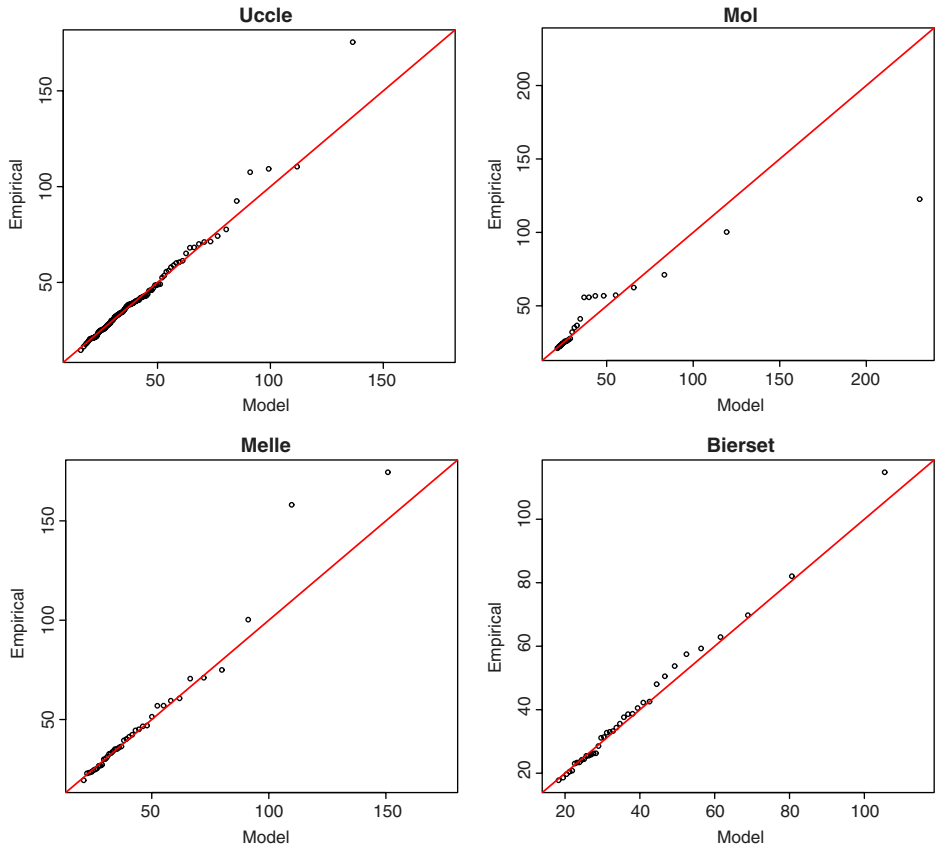

Figure 5. Quantile plots of the GEV fit to precipitation deficit maxima (mm) for grass, for Uccle (1901–2005), Mol (1967–1996), Melle and Bierset (1967–2005).

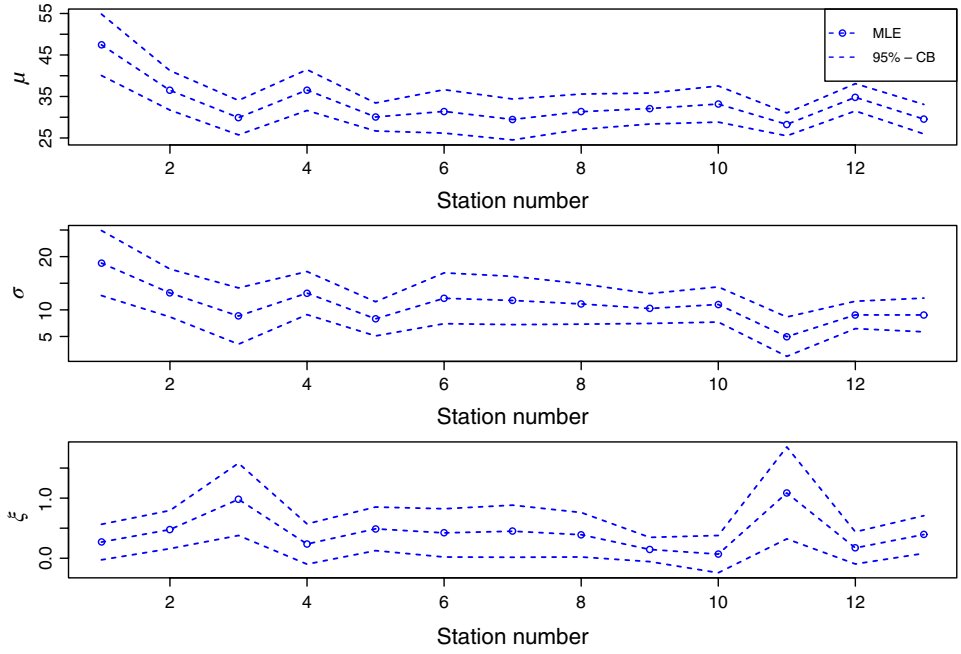

Figure 6. Stationwise MLEs of GEV-parameters for maximum precipitation deficit (cover type: deciduous forest) (see Table 1 for station numbers).

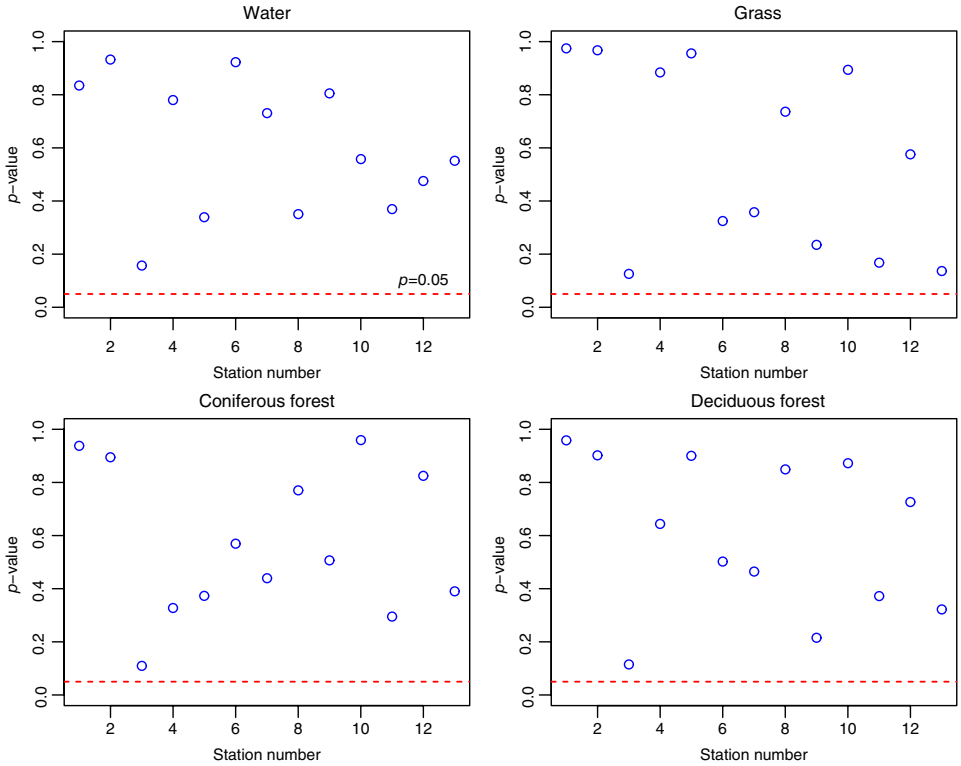

Figure 7. *p*-Values of Cramer–von Mises goodness of fit test (Laio, 2004) for the GEV-distribution (see Table 1 for station numbers).

$\mu(r)$, but have constant $\sigma(r) = \sigma_0$. Models $M_6, \ldots, M_{10}$ include a covariate in both $\mu(r)$ and $\sigma(r)$. The TIC-values (Table 2) confirm the ability of the covariates to capture the spatial variability. The models $M_6, \ldots, M_{10}$ are superior to the intermediate models $M_1, \ldots, M_5$. Increasing model complexity by adding more than one covariate in the GEV-parameters, as with models M_{11} and M_{12}, does not improve model's performance (in TIC terms).

For the strongest model (M_{10}), the MLE $\hat{\xi}$ and associated standard errors computed with Equation (11) are

$$\hat{\xi}_W = 0.299\ (0.127)\,, \hat{\xi}_G = 0.314\ (0.121)\,,$$
$$\hat{\xi}_{CF} = 0.318\ (0.123)\,, \hat{\xi}_{DF} = 0.320\ (0.122) \qquad (14)$$

However, the actual ξ-estimates result in intersecting return level plots, which is physically not consistent.

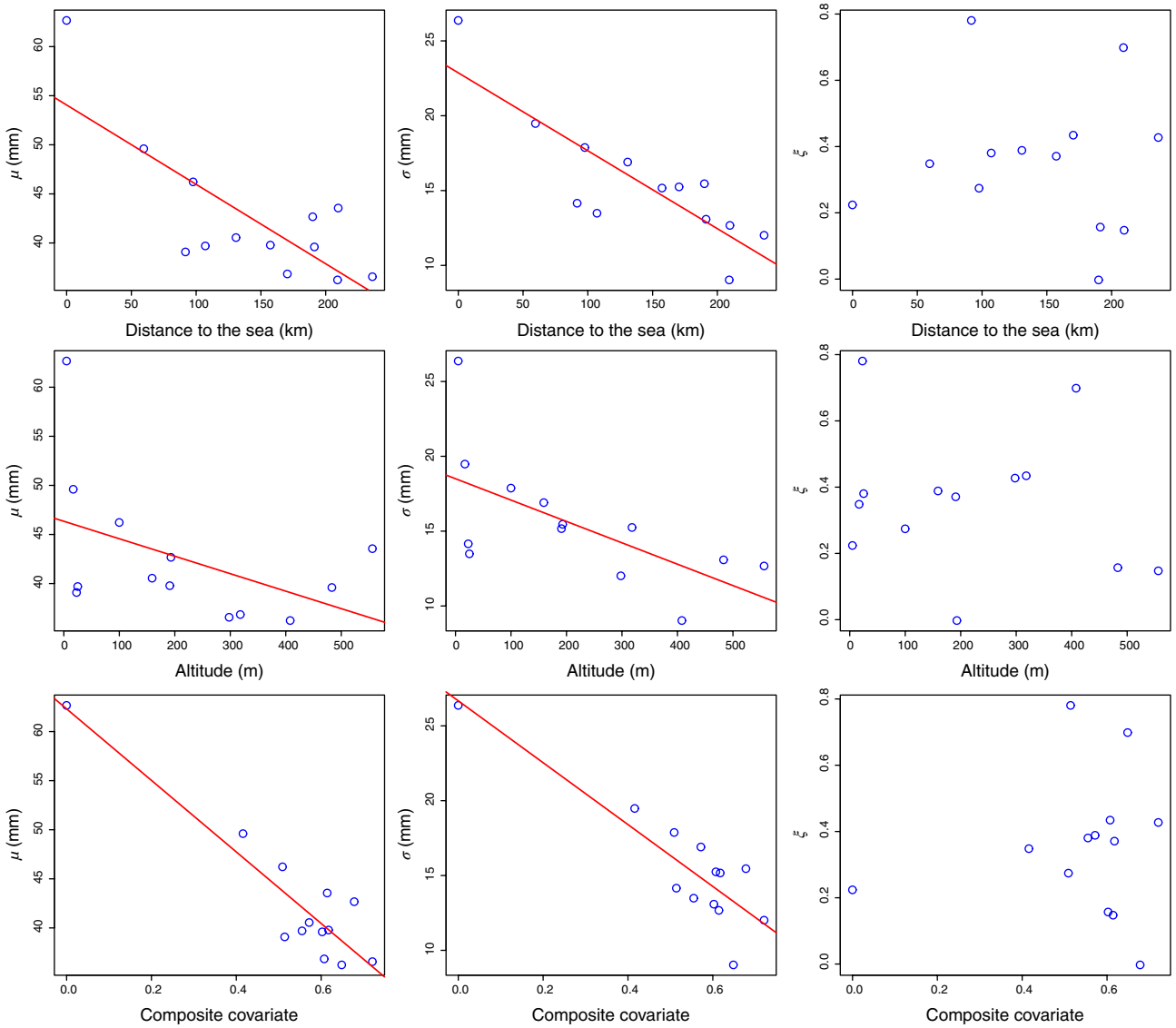

Figure 8. Scatter plot of stationwise GEV-parameters against different covariates (cover type: water). Solid line: best fitting straight line.

For example, the return levels for water must be higher than those for grass. For $\widehat{\mu}_W(r) > \widehat{\mu}_G(r)$, and $\widehat{\sigma}_W(r) > \widehat{\sigma}_G(r)$, the return level plots will not intersect if $\widehat{\xi}_W \geq \widehat{\xi}_G$. In order to avoid intersection, we keep the value of ξ fixed for the four cover types, $\xi = 0.31$. The parameters $\mu^{(0)}$, $\mu^{(1)}$, $\sigma^{(0)}$, $\sigma^{(1)}$ are subsequently re-estimated (Table 3), and we can maintain the estimated variance/covariance matrix of the original estimation.

Return level maps for any return period can be computed with Equation (6). At each grid point r_i, the estimated GEV parameters are $\widehat{\mu}(r_i) = \widehat{\mu}^{(0)} + \widehat{\mu}^{(1)} C(r_i)$, $\widehat{\sigma}(r_i) = \widehat{\sigma}^{(0)} + \widehat{\sigma}^{(1)} C(r_i)$ and $\xi = 0.31$ (cfr. Equation (9)), for which covariate information, $C(r_i)$, can be obtained from digital terrain models. GTOPO30, for example, provides a global digital elevation model and is freely available (USGS, 1996). In Figure 9 (left column), we have plotted 20-year return level maps of precipitation deficit (four cover types), provided by the smooth spatial GEV model using the strongest covariate, $\sqrt{D/(a_0 + a_1 H)}$. The grid resolution is 4×4 km, which is in keeping with current state-of-the-art regional climate models (Hamdi *et al.*, 2012). The maps indicate that the model is able to reproduce reasonable values and a similar spatial pattern to the map of mean annual evaporation (Gellens-Meulenberghs and Gellens, 1992). The largest values occur along the coast, while the lowest values are in the hilly region of the south-east. A great advantage of MLE is that the standard errors of the spatial return level estimates can be immediately calculated with the well-known *delta method* (Coles, 2001). The bounds of the 95% confidence intervals are shown in Figure 9 (middle and right column).

4.4. Predictive comparison

The quality of the spatial predictions was assessed with several model performance scores which are based

Table 2. TIC-values of spatial GEV-models of the form Equation (9), with $\xi(r) = \xi_0$.

	GEV-model	W	G	CF	DF
M_0:	$\mu(r) = \mu_0$ $\sigma(r) = \sigma_0$	4667.77	4212.62	4481.53	4355.47
M_1:	$\mu(r) = \mu_0 + \mu_1$ LON $\sigma(r) = \sigma_0$	4661.45	4206.98	4477.14	4350.71
M_2:	$\mu(r) = \mu_0 + \mu_1$ LAT $\sigma(r) = \sigma_0$	4663.16	4207.61	4476.52	4351.30
M_3:	$\mu(r) = \mu_0 + \mu_1 H$ $\sigma(r) = \sigma_0$	4667.78	4211.81	4481.65	4355.43
M_4:	$\mu(r) = \mu_0 + \mu_1 D$ $\sigma(r) = \sigma_0$	4658.83	4202.90	4473.01	4347.19
M_5:	$\mu(r) = \mu_0 + \mu_1 \sqrt{\frac{D}{a_0 + a_1 H}}$ $\sigma(r) = \sigma_0$	4648.75	4192.91	4464.41	4337.94
M_6:	$\mu(r) = \mu_0 + \mu_1$ LON $\sigma(r) = \sigma_0 + \sigma_1$ LON	4651.75	4202.64	4468.43	4346.48
M_7:	$\mu(r) = \mu_0 + \mu_1$ LAT $\sigma(r) = \sigma_0 + \sigma_1$ LAT	4653.90	4203.03	4469.61	4345.47
M_8:	$\mu(r) = \mu_0 + \mu_1 H$ $\sigma(r) = \sigma_0 + \sigma_1 H$	4662.52	4212.58	4478.75	4355.75
M_9:	$\mu(r) = \mu_0 + \mu_1 D$ $\sigma(r) = \sigma_0 + \sigma_1 D$	4648.42	4198.56	4464.85	4342.11
M_{10}:	$\mu(r) = \mu_0 + \mu_1 \sqrt{\frac{D}{a_0 + a_1 H}}$ $\sigma(r) = \sigma_0 + \sigma_1 \sqrt{\frac{D}{a_0 + a_1 H}}$	**4635.94**	**4184.37**	**4451.21**	**4327.50**
M_{11}:	$\mu(r) = \mu_0 + \mu_1 \sqrt{\frac{D}{a_0 + a_1 H}} + \mu_2$ LON $\sigma(r) = \sigma_0 + \sigma_1 \sqrt{\frac{D}{a_0 + a_1 H}}$	4637.21	4187.65	4452.65	4330.31
M_{12}:	$\mu(r) = \mu_0 + \mu_1 \sqrt{\frac{D}{a_0 + a_1 H}} + \mu_2$ LON $\sigma(r) = \sigma_0 + \sigma_1 \sqrt{\frac{D}{a_0 + a_1 H}} + \sigma_2$ LON	4639.15	4189.41	4455.03	4332.13

Best performing models are indicated in bold.

Table 3. MLEs $\widehat{\mu}^{(0)}$, $\widehat{\mu}^{(1)}$, $\widehat{\sigma}^{(0)}$, $\widehat{\sigma}^{(1)}$ and the associated standard errors (in parentheses) of the spatial GEV model M_{10} (see Table 2), with $\xi = 0.31$.

Cover type	$\widehat{\mu}^{(0)}$ (mm)	$\widehat{\mu}^{(1)}$ (−)	$\widehat{\sigma}^{(0)}$ (mm)	$\widehat{\sigma}^{(1)}$ (−)
Water	61.88 (4.47)	−35.03 (5.49)	26.96 (3.43)	−19.76 (4.32)
Grass	40.87 (2.38)	−20.28 (2.84)	15.87 (2.09)	−10.28 (2.83)
Coniferous forest	52.31 (3.43)	−28.11 (4.11)	22.22 (2.83)	−16.20 (3.54)
Deciduous forest	46.36 (2.80)	−23.48 (3.39)	18.82 (2.44)	−12.88 (3.20)

on a comparison between observed and predicted values. Suppose we have annual maxima data z_{ij} at a given station $i = 1, \ldots, n$, and a spatial estimator GEV $[\widehat{\mu}(r), \widehat{\sigma}(r), \widehat{\xi}]$. We compute goodness-of-fit scores with the *leaving-one-out* methodology which means that the observations of the ith station are removed, and the spatial model is estimated on the remaining data. The predicted values from GEV $\left[\widehat{\mu}(r_i), \widehat{\sigma}(r_i), \widehat{\xi}\right]$ are compared with the observations of the ith station, and the whole methodology is repeated for each station $i = 1, \ldots, n$.

Four goodness-of-fit scores were used: the root mean square error (RMSE), the mean absolute error (MAE), the maximum prediction error (MPE), and the bias. Let $z_{i(1)} \leq \ldots \leq z_{i(k)}$ be the sorted annual maxima z_{ij} at a given station i. As for sitewise GEV estimations (Section 4.2), the empirical probability $p_j = P\{z < z_{i(j)}\}$ is approximated by the Weibull plotting position. $z_{i(j)}$ can be compared with the p_j-quantile of GEV $\left[\widehat{\mu}(r_i), \widehat{\sigma}(r_i), \widehat{\xi}\right]$, here denoted by q_{ij}. The latter is given by Equation (6), where μ and σ are replaced by spatially modelled values $\widehat{\mu}(r_i)$ and $\widehat{\sigma}(r_i)$, and where T is replaced by the empirical return period $1/(1 - p_j)$:

$$q_{ij} = \widehat{\mu}(r_i) - \frac{\widehat{\sigma}(r_i)}{\widehat{\xi}} \left\{1 - \left[-\log(p_j)\right]^{-\widehat{\xi}}\right\} \qquad (15)$$

The scores for quantile comparison at the ith station ($z_{i(j)}$ *vs* q_{ij}) are then given by

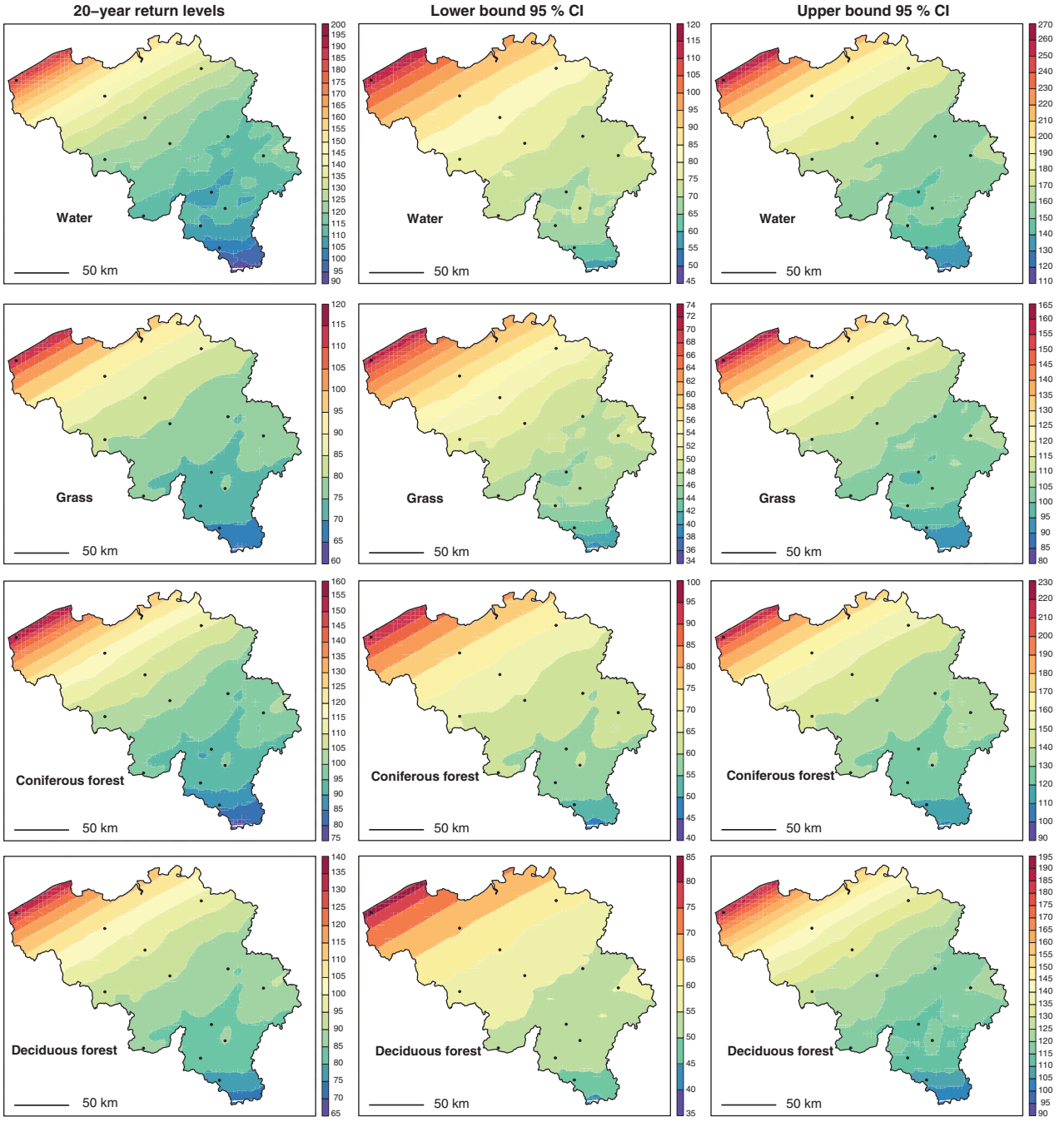

Figure 9. 20-Year return level maps, and bounds of the 95% confidence intervals (CI) for precipitation deficit (mm), obtained by the spatial GEV model M_{10} (see Table 2).

$$\begin{aligned}
\mathrm{RMSE}_i &= \left(\frac{1}{k}\sum_{j=1}^{k}\left(z_{i(j)}-q_{ij}\right)^2\right)^{1/2},\\
\mathrm{MAE}_i &= \frac{1}{k}\sum_{j=1}^{k}\left|z_{i(j)}-q_{ij}\right|,\\
\mathrm{MPE}_i &= \max_{j\in\{1,\ldots,k\}}\left|z_{i(j)}-q_{ij}\right|,\\
\mathrm{BIAS}_i &= \frac{1}{k}\sum_{j=1}^{k}\left(z_{i(j)}-q_{ij}\right)
\end{aligned} \tag{16}$$

As a reference, we compare the scores corresponding to fitting a GEV distribution to each station separately, without any spatial model. For the sitewise distribution GEV $\left[\widehat{\mu}_i,\widehat{\sigma}_i,\widehat{\xi}_i\right]$, the p_j-quantile is

$$q^*_{ij}=\widehat{\mu}_i-\frac{\widehat{\sigma}_i}{\widehat{\xi}_i}\left\{1-\left[-\log\left(p_j\right)\right]^{-\widehat{\xi}_i}\right\},$$

and the corresponding scores are obtained when replacing q_{ij} by q^*_{ij} in Equation (16).

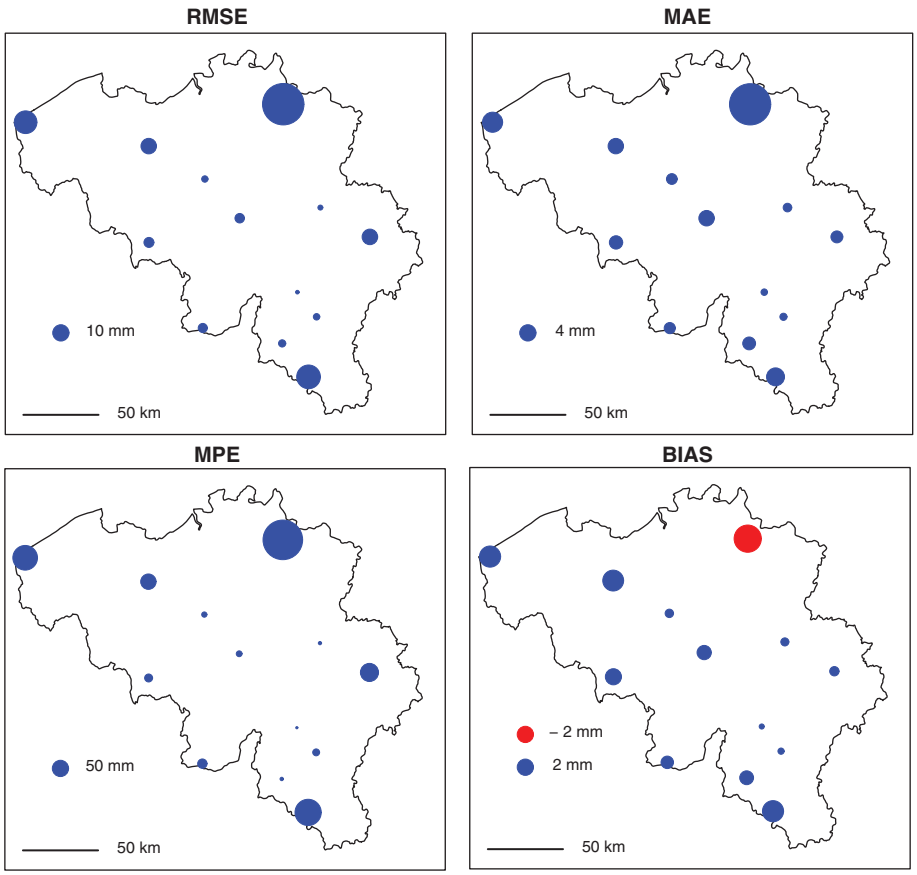

Figure 10. Goodness-of-fit scores. Sitewise GEV distribution (coniferous forest).

The scores for the sitewise GEV model, and the smooth spatial GEV model are displayed in Figures 10 and 11 in the case of coniferous forest. It can be seen that the sitewise GEV fit for station Mol is not satisfactory. Specifically, the MPE value, Equation (16), is very large, due to large estimation errors of ξ which produce strong overestimations of the largest observations. With the exception of station Mol, the sitewise estimator performs better than the spatial estimator.

An overall picture of the goodness-of-fit can be obtained by averaging the sitewise scores, Equation (16), over n stations. We get the following overall scores:

$$\mathrm{RMSE} = \left(\frac{1}{n}\sum_{i=1}^{n}\mathrm{RMSE}_i^2\right)^{1/2}, \mathrm{MAE} = \frac{1}{n}\sum_{i=1}^{n}\mathrm{MAE}_i,$$

$$\mathrm{MPE} = \frac{1}{n}\sum_{i=1}^{n}\mathrm{MPE}_i. \qquad (17)$$

The overall scores, Equation (17), indicates that the sitewise estimator performs slightly better than the spatial estimator (Table 4). In view of this promising result, there are enough grounds to support the use of spatial models for extremes in regional drought studies.

In Figure 12 we plotted the 20-year return levels of the sitewise and the smooth spatial GEV model. This comparison is between two estimators, and not between an estimator and an observation. Therefore, we have added the observed 20-year return levels to the plots, which were computed using ranking. The ranks j_{20} and $j_{20}+1$ of $z_{i(1)} \leq \ldots \leq z_{i(k)}$, which are closest to the observed 20-year return level, can be found by solving the inequalities, $p_j \leq 1 - 1/20 \leq p_{j+1}$, to j. The observed 20-year return level is then derived by linear interpolation from $z_{i(j_{20})}$ and $z_{i(j_{20}+1)}$. All the plots agree with the goodness-of-fit scores of Figures 10 and 11.

5. Discussion

This work highlights the benefit of EVT for drought studies. The precipitation deficit is defined as a rainfall-evapotranspiration balance, and the summer half-year maxima (1 April–30 September) are used to identify droughts. The PET-data were calculated from 13 weather stations across Belgium. We applied our methods to data recorded during the years 1967–2005, except for the Uccle data which cover the years 1901–2005. The stationarity of the precipitation deficit maxima series, a common assumption in many time series techniques, was confirmed with the Mann–Kendall trend test. In addition, the time-independence of the series was confirmed with the autocorrelation function.

The GEV distribution could be successfully fitted to maximum precipitation deficits, despite the fact that daily observations are not independent and identically

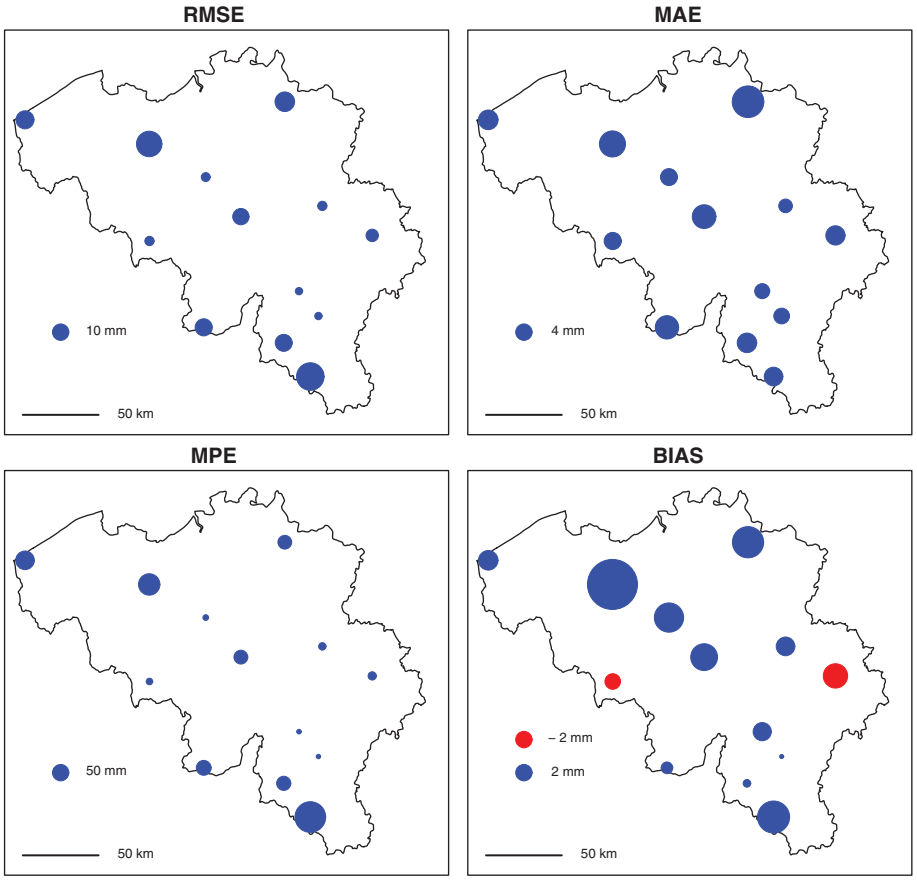

Figure 11. Goodness-of-fit scores. Spatial GEV model M_{10}, see Table 2 (coniferous forest).

Table 4. Scores of quantile comparison when (a) fitting a GEV to each station separately; and (b) spatial GEV modelling with M_{10} (see Table 2).

	Water			Grass		
	RMSE	MAE	MPE	RMSE	MAE	MPE
(a) Sitewise GEV	9.50	3.93	39.12	9.31	3.09	36.22
(b) Smooth GEV	10.57	5.52	39.53	8.55	3.86	33.18
	Coniferous forest			Deciduous forest		
	RMSE	MAE	MPE	RMSE	MAE	MPE
(a) Sitewise GEV	10.39	3.64	39.75	9.47	3.31	37.43
(b) Smooth GEV	9.97	4.88	38.56	9.71	4.51	38.44

Unit of the scores is mm.

distributed. However, for a large number of classes of dependent sequences, EVT can be applied for descriptive or predictive purposes (Leadbetter *et al.*, 1983). To date only Beersma and Buishand (2004, 2007) applied EVT to model precipitation deficit which they defined as the difference between precipitation and evaporation. Return level estimations based on the GEV distribution for extreme precipitation deficit are particularly useful for insurances as they provide information on the probability of occurrence and the associated magnitude of drought.

An important statistical contribution of this work lies in the development and application of extreme value analysis yielding return level maps of precipitation deficit for water, grass, coniferous and deciduous forest. Spatial modelling of precipitation deficit in the context of extremes is unprecedented and allows to define extreme value distributions across a region on the basis of carefully selected covariates. By performing the spatial analysis on locations defined by covariates, we are able to model regional differences in extreme precipitation deficit. The composite covariate $\sqrt{D/\left(a_0 + a_1 H\right)}$ ($a_0 = 337.98$, $a_1 = 0.39$) provides the best fits with the advantage that elevations (H) and distances to the sea (D) are available at a regular grid to represent a continuous surface. The modelling of the GEV-parameters is based on linear relationships with the covariates. A smooth spatial structure is an intrinsic feature of the model. Introducing several degrees of complexity

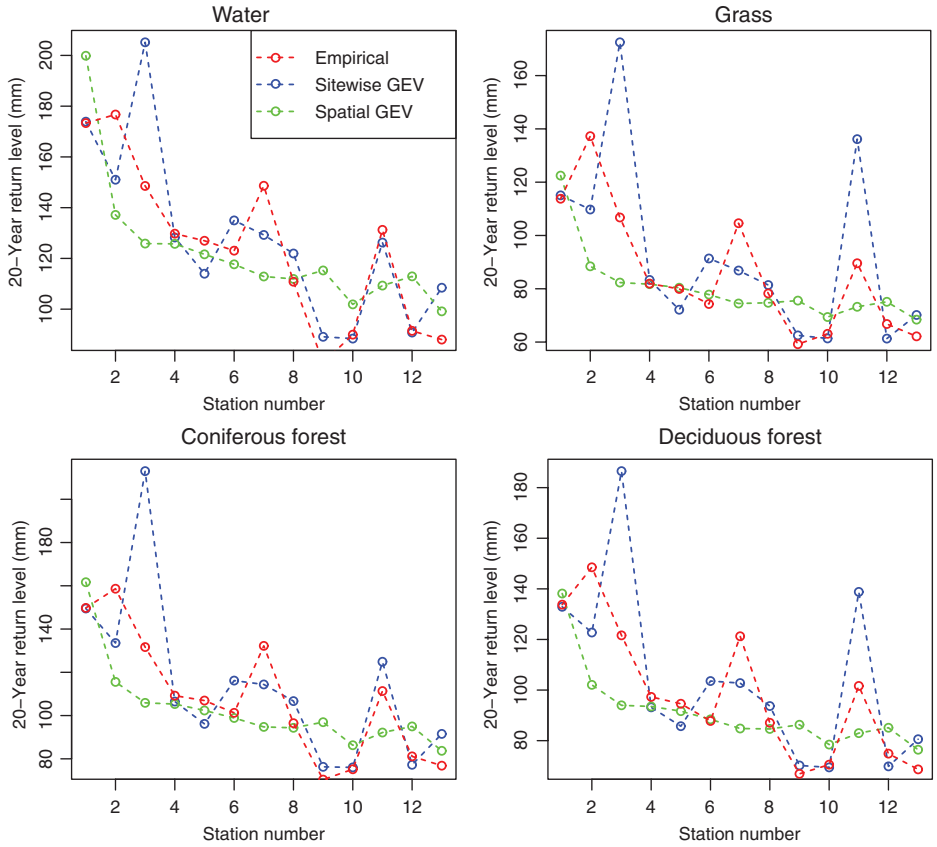

Figure 12. The 20-year return levels of maximum precipitation deficit (mm). GEV-models *versus* observations.

and non-linearity in covariate dependent modelling is possible, provided the availability of gridded covariate data. However, for a fit to 13 sites we restricted the development to parsimonious models. A constant shape parameter is a common assumption in smooth spatial GEV modelling (Gellens, 2002; Cooley *et al.*, 2007; Sang and Gelfand, 2009; Blanchet and Lehning, 2010; Padoan *et al.*, 2010; Northrop and Jonathan, 2011; Westra and Sisson, 2011; Van de Vyver, 2012; Dyrrdal *et al.*, 2015). The smooth spatial GEV model combines data from single sites so that the estimation errors can be obtained directly. The overall scores of the spatial models are promising because they do not differ that much from the goodness-of-fit scores of the sitewise GEV model.

This analysis can be extended in various ways. A measure of drought severity can be refined by quantifying the precipitation deficit for multiple time scales. The use of multivariate extreme value analysis is particularly attractive in this context (Beirlant *et al.*, 2004). The definition of precipitation deficit can be extended to include soil moisture or vegetation performance (Williams *et al.*, 2012), or in an operational context to estimate return periods from extreme deficits and vice versa.

6. Conclusions

Quantitative indicators are important for an overall perspective on drought over a region. We defined precipitation deficit as a cumulative difference between precipitation and evapotranspiration for water, grass, coniferous and deciduous forest. The highest deficits invariably occur during the summer half year (April–September) and are stationary during the observation period. Smooth spatial GEV modelling using linear relationships between GEV parameters and a composite geographical covariate comprising elevation and distance to the sea allowed for direct estimations of return levels and associated errors. Model performance metrics and statistical scores for spatial GEV modelling were similar to sitewise GEV models, but the sitewise GEV models fit the observations better. Smooth spatial GEV modelling can overcome datasets with a poor spatial coverage because information transfer between sites allows for improved inferences. The model development can therefore be extended to include closely linked features such as moisture deficit or to explore vegetation performance and vulnerability.

Acknowledgements

This work is supported by the Belgian Science Policy Office (BELSPO) under Contract No. SD/RI/03A. We are grateful to Dr T.A. Buishand (KNMI) and Dr E. Roulin (RMI) whose helpful comments and suggestions seriously improved this paper. We are particularly indebted to M. Journée and C. Trapenard (RMI) for delivering the evapotranspiration data.

References

Beersma J, Buishand T. 2004. Joint probability of precipitation and discharge deficits in the Netherlands. *Water Resour. Res.* **40**: W12508, doi: 10.1029/2004WR003265.

Beersma J, Buishand T. 2007. Drought in the Netherlands – regional frequency analysis versus time series simulation. *J. Hydrol.* **347**: 332–346, doi: 10.1016/j.jhydrol.2007.09.042.

Beirlant J, Goegebeur Y, Seger J, Teugels J. 2004. *Statistics of Extremes*. John Wiley & Sons, Ltd: Chichester, UK.

Beran, M. and Rodier, J. (1985). Hydrological aspects of drought. *Studies and Reports in Hydrology*, Report no. 39, UNESCO-WMO, Paris, France.

Blanchet J, Lehning M. 2010. Mapping snow depth return levels: smooth spatial modelling versus station interpolation. *Hydrol. Earth Syst. Sci.* **14**: 2527–2544, doi: 10.5194/hess-14-2527-2010.

Bleiman N. 1976. *Estimation des valeurs journalières de l'évaporation d'une nappe d'eau libre et de l'évapotranspiration potentielle du gazon à Uccle (50°48′, 4°21′, 100 m) pour la période 1901–1975*. Issue 5 of Miscellanea Série A. Royal Meteorological Institute of Belgium: Bruxelles.

Brouyaux F, Tricot C, Debontridder L, Delcloo A, Vandiepenbeek M, Dewitte S, Cheymol A, Joukoff A, De Backer H, Hus J, Van Malderen R, Vannitsem S, Roulin E, Mohymont B. 2008. *Oog voor het klimaat/Vigilance climatique*. Royal Meteorological Institute of Belgium: Bruxelles.

Bultot F, Dupriez G. 1973. L'évaporation d'un bac de d'eau libre – sa signification restreinte. *J. Hydrol.* **20**: 83–95, doi: 10.1016/0022-1694(73)90046-2.

Bultot F, Coppens A, Dupriez G. 1983. *Estimation de l'évapotranspiration potentielle en Belgique (procédure révisée)*. Issue 12 of Publications Série A. Royal Meteorological Institute of Belgium: Bruxelles.

Bultot F, Dupriez G, Gellens D. 1988. Estimated annual regime of energy balance components, evapotranspiration and soil moisture for a drainage basin in case of a CO_2 doubling. *Clim. Change* **12**: 39–56, doi: 10.1007/BF00140263.

Chandler R, Bate S. 2007. Inference for clustered data using the independence log-likelihood. *Biometrika* **94**: 167–183, doi: 10.1093/biomet/asm015.

Coles S. 2001. *An Introduction to Statistical Modeling of Extreme Values*. Springer-Verlag, London Ltd.: London.

Cooley D, Nychka D, Naveau P. 2007. Bayesian spatial modeling of extreme precipitation return levels. *J. Am. Stat. Assoc.* **102**: 824–840, doi: 10.1198/016214506000000780.

Demarée G. 2003. Le pluviographe centenaire du plateau d'Uccle: son histoire, ses données et ses applications. *La Houille Blanche* **4**: 95–102, doi: 10.1051/lhb/2003082.

Dracup J, Lee K, Paulson J. 1980. On the definition of drought. *Water Resour. Res.* **16**: 297–302, doi: 10.1029/WR016i002p00289.

Dyrrdal A, Lenkoski A, Thorarinsdottir T, Stordal F. 2015. Bayesian hierarchical modeling of extreme hourly precipitation in Norway. *Environmetrics* **26**: 89–106, doi: 10.1002/env.2301.

FAO. 1978. Report on the Agro-ecological Zones Project. vol. 1, *Methodology and Results for Africa*, FAO World Soil Resources Report 48/1.

Gellens D. 2002. Combining regional approach and data extension procedure for assessing GEV distribution of extreme precipitation in Belgium. *J. Hydrol.* **268**: 113–126.

Gellens-Meulenberghs F, Gellens D. 1992. *L'évaporanspiration potentielle en Belgique: variabilite spatiale et temporelle*. Issue 130 of Publications Série A. Royal Meteorological Institute of Belgium: Bruxelles.

Goegebeur Y, Planchon V, Beirlant J, Oger R. 2005. Quality assessment of pedochemical data using extreme value methodology. *J. Appl. Sci.* **5**: 1092–1102, doi: 10.3923/jas.2005.1092.1102.

Hamdi R, Van de Vyver H, Termonia P. 2012. New cloud and microphysics parameterisation for use in high-resolution dynamical downscaling: application for summer extreme temperature over Belgium. *Int. J. Climatol.* **32**: 2051–2065, doi: 10.1002/joc.2409.

Hiemstra P, Sluiter R. 2011. Interpolation of Makkink evaporation in the Netherlands. Technical Report TR-327, Royal Netherlands Meteorological Institute, De Bilt, The Netherlands.

Hisdal H, Stahl K, Tallaksen L, Demuth S. 2001. Have streamflow droughts in Europe become more severe or frequent? *Int. J. Climatol.* **21**: 317–333, doi: 10.1002/joc.619.

Katz R, Parlange M, Naveau P. 2002. Statistics of extremes in hydrology. *Adv. Water Resour.* **25**: 1287–1304, doi: 10.1016/S0309-1708(02)00056-8.

Kingston D, Todd M, Taylor R, Thompson J, Arnell N. 2009. Uncertainty in the estimation of potential evapotranspiration under climate change. *Geophys. Res. Lett.* **36**: L20403, doi: 10.1029/2009GL040267.

Laio F. 2004. Cramer-von Mises and Anderson-Darling goodness of fit test for extreme value distributions with unknown parameters. *Water Resour. Res.* **40**: W09308, doi: 10.1029/2004WR003204.

Leadbetter M, Lindgren G, Rootzén H. 1983. *Extremes and Related Properties of Random Sequences and Processes*. Springer-Verlag: New York, NY and Heidelberg, Berlin.

Maracchi G, Sirotenko O, Bindi M. 2005. Impacts of present and future climate variability on agriculture and forestry in the temperate regions: Europe. *Clim. Change* **70**: 117–135, doi: 10.1007/1-4020-4166-7-6.

McLeod A. 2011. *Kendall: Kendall Rank Correlation and Mann-Kendall Trend Test. R package version 2.2*.

Monteith J. 1973. *Principles of Environmental Physics*. Edward Arnold: London.

Naveau P, Nogaj M, Ammann C, Yiou P, Cooley D, Jomelli V. 2005. Statistical analysis of climate extremes. *C R Acad Sci II A* **337**: 1013–1022, doi: 10.1016/j.crte.2005.04.015.

Northrop P, Jonathan P. 2011. Threshold modelling of spatially dependent non-stationary extremes with application to hurricane-induced wave heights. *Environmetrics* **22**: 799–809, doi: 10.1002/env.1106.

Olesen J, Bindi M. 2002. Consequences of climate change for European agricultural productivity, land use and policy. *Eur. J. Agron.* **16**: 239–262, doi: 10.1016/S1161-0301(02)00004-7.

Orlandini S, Nejedlik P, Eitzinger J, Alexandrov V, Toulios L, Calanca P, Trnka M, Olesen J. 2008. Impacts of climate change and variability on European agriculture: results of inventory analysis in COST 734 countries. *Ann. N. Y. Acad. Sci.* **1146**: 338–353, doi: 10.1196/annals.1446.013.

Padoan S, Ribatet M, Sisson S. 2010. Likelihood-based inference for max-stable processes. *J. Am. Stat. Assoc.* **105**: 263–277.

Penman H. 1948. Natural evaporation from open water, bare soil, and grass. *Proc. R. Soc. Lond. A* **193**: 120–146, doi: 10.1098/rspa.1948.0037.

Reidsma P, Ewert F, Lansink A, Leemans R. 2009. Vulnerability and adaptation of European farmers: a multi-level analysis of yield and income responses to climate variability. *Reg. Environ. Change* **9**: 25–40, doi: 10.1007/s10113-008-0059-3.

Rossi G. 2000. Drought mitigation measures: a comprehensive framework. In *Drought and Drought Mitigation in Europe*, Voght J, Somma F (eds). Kluwer Academic Publishers: Dordrecht, The Netherlands, 233–246.

Rossi G, Benedini M, Tsakiris G, Giakoumakis S. 1992. On regional drought estimation and analysis. *Water Resour. Manag.* **6**: 249–277, doi: 10.1007/BF00872280.

Rotnitzky A, Jewell N. 1990. Hypothesis testing of regression parameters in semiparametric generalized linear models for cluster correlated data. *Biometrika* **77**: 485–497, doi: 10.1093/biomet/77.3.485.

Sang H, Gelfand A. 2009. Hierarchical modeling for extreme values observed over space and time. *Environ. Ecol. Stat.* **16**: 407–426, doi: 10.1007/s10651-007-0078-0.

Stephenson A. 2012. *ISMEV: An Introduction to Statistical Modeling of Extreme Values* Original S functions written by Janet E. Heffernan with R port and R documentation provided by Alec G. Stephenson. R package version 1.39.

Takeuchi K. 1976. Distribution of informational statistics and a criterion of model fitting. *Math. Sci.* **153**: 12–18.

Tallaksen L, Hisdal H. 1997. Regional analysis of extreme streamflow drought duration and deficit volume. In *Friend '97 – Regional Hydrology: Concepts and Models for Sustainable Water Resource Management*, Gustard A, Blazkova S, Brilly M, Demuth S, Dixon J, van Lanen H, Llasat C, Mkhandi S, Servat E (eds). IAHS Press: Wallingford, UK, 141–150.

USGS. 1996. Global 30 Arc-Second Elevation Dataset (GTOPO30). http://eros.usgs.gov (accessed 15 May 2014).

Van de Vyver H. 2012. Spatial regression models for extreme precipitation in Belgium. *Water Resour. Res.* **48**: W09549, doi: 10.1029/2011WR011707.

Varin C. 2008. On composite marginal likelihoods. *Adv. Stat. Anal.* **92**: 1–28.

Westra S, Sisson S. 2011. Detection of non-stationarity in precipitation extremes using a max-stable process model. *J. Hydrol.* **406**: 119–128.

Wilhite D, Glantz M. 1985. Understanding the drought phenomenon: the role of definitions. *Water Int.* **10**: 111–120, doi: 10.1080/02508068508686328.

Williams C, Reichstein M, Buchmann N, Baldocchi D, Beer C, Schwalm C, Wohlfahrt G, Hasler N, Bernhofer C, Foken T, Papale D, Schymanski S, Schaefer K. 2012. Climate and vegetation controls on the surface water balance: synthesis of evapotranspiration measured across a global network of flux towers. *Water Resour. Res.* **48**: W06523, doi: 10.1029/2011WR011586.

Zheng F, Thibaud E, Leonard M, Westra S. in press. Assessing the performance of the independence method in modeling spatial extreme rainfall. *Water Resour. Res.* (in press).

